

# Investigation on stress micro-cycles and mild wear mechanism in gear contact fatigue

Ye Zhou<sup>a,b</sup>, Caichao Zhu<sup>a</sup>, Huaiju Liu<sup>a</sup>, Houyi Bai<sup>c</sup>, Xiaona Xu<sup>c</sup>

<sup>a</sup> State Key Laboratory of Mechanical Transmissions, Chongqing University, Chongqing 400030, China

<sup>b</sup> College of Aerospace Engineering, Chongqing University, Chongqing 400044, China

<sup>c</sup> Chongqing Wangjiang Industrial Co., Chongqing 400071, China

\*Corresponding author: [zhouye@cqu.edu.cn](mailto:zhouye@cqu.edu.cn)

**Abstract :** Gear contact fatigue is becoming a primary limitation for the growing demand of power density and service life in gear-driven equipment. The unchecked surface fatigue crack could further cause premature failure and put a serious risk to the safety and reliability of mechanical systems. In this work, an attempt is made to investigate the effects of rolling-sliding and mild wear on contact fatigue behavior. A comprehensive contact model is developed to capture the variation instantaneous pressure and stress field is calculated with the transient mixed EHL approach. Rolling-sliding contact is simulated with the time-varying roughness topography updated by Archard wear equation. The stress cycles are extracted and the relative contact fatigue life is obtained by using Zaretsky criterion. Results suggest that in rolling-sliding contact the contact fatigue life is obviously lower compared with pure rolling. The increases in the number and amplitude of stress micro-cycles is found to be the main contributors to the reduction of fatigue life. Mild wear tends to smooth the surface, subsequently mitigates the stress concentration and reduces stress cycles, then decrease the risk of surface contact fatigue.

**Keywords:** Gear contact fatigue; mild wear; rolling-sliding contact; stress micro-cycles; mixed EHL

## 1. Introduction

The premature surface failure caused by gear contact fatigue severely restricts the power density, reliability and service life of modern mechanical systems. The unchecked surface crack could further cause micropitting, pitting and spalling, etc., which put a serious risk to the safety and reliability of gear-driven equipment, as reported in wind turbine and helicopter accidents [1, 2]. Traditional gear contact fatigue design method is based upon the Hertzian

contact theory and the simplex mapping process from stress to life under quasi-static conditions [3]. However, the mixed rolling-sliding motion takes a complex condition on contact interfaces: in a macro sense, the kinematic sliding changes the distribution of surface tractions, while the interaction between micro asperities and lubricants introduces the stress fluctuation. In addition, the variation of surface topography under cyclic loading leads to the evolution of contact performance. Due to the complicated contact characteristics and intricate correlation between mild wear and surface contact fatigue, the evolution rule and coupling mechanism of gear contact performance remains mostly unknown.

Owing to the development of mixed EHL and DC-FFT algorithm, lubricated rough surface contact can be well modeled and solved. Over the last decade, gear contact fatigue was extensively studied with EHL theory and various fatigue models. Based on the idea of failure probability, Zhu et al. [4] calculated surface pitting life using von Mises stress. The predicted results agree well with tests after adjusting stress exponent in the life model. The study pointed out gear tooth surface finishing significantly effects contact fatigue life. Li and Kahraman [5] combined stress field and multi-axial fatigue criterion to develop a gear micropitting model, which can predict both the crack nucleation fatigue life and the depth of the critical failure sites. Evans et al. [6] analyzed the gear surface fatigue damage by using the Palmgren-Miner damage accumulation rule. The damage distribution is represented by Weibull cumulative density function, which can depict the damage at different depths. The aforementioned models represent three typical approaches to evaluate gear contact fatigue performance under mixed lubrication state. Following these approaches, the influences of tribo-dynamic characteristic [7], surface topography [8], case-hardening property [9] and material inclusion [10] on gear contact fatigue were extensively investigated. However, most of the studies were based on the simulation of a single meshing cycle, in which the roughness profile and stress field were assumed to be invariable. The variations of surface topography during the rolling-sliding contact and cyclic loading were ignored.

The special attention was given to correlation between gear contact fatigue and surface mild wear can be traced back to the experimental work of Laine et al. [11]. By using zinc dialkyldithio-phosphate (ZDDP) anti-wear additive, they found an approximately converse

trend between micropitting damage rate and mild wear in benchtop tests. Brandao et al. [12] investigated surface damage and mass loss through FZG gear test and simulation. They suggested a wear process should be included to evaluate the overall change of tooth flank profile. Based on the ideal of mild wear, Morales-Espejel et al. [13, 14] reported a numerical model incorporating the evolution of roughness profile and surface fatigue damage, and subsequently predicted micropitting damage risk on tooth flank. Guilbault and Lalonde [15] statistically investigated the evolution of asperity shape caused by surface wear under mixed lubrication, then predicted the crack initiation by using damage accumulation procedure and multiaxial fatigue criterion. Most recently, Liu et al. [16] reported the change of failure mode caused by the roughness variation through identifying the critical damage position. These researches indicated that mild wear is of great importance in the fatigue analysis. Most of them just focus on the constant contact state, while the influence of time-varying stress cycle is neglected. To count the stress cycles introduced by the rough sliding contact, Pu et al. [17] derived a statistical formula based on the assumed sinusoidal roughness. Zhou et al. [18] developed a numerical model incorporating the stress micro-cycles based on rain-flow counting method. However, the impact of rolling-sliding on gear contact fatigue remains obscure. It should be considered that the kinematic sliding takes new surface topography into contact in the numerical simulation.

When analyzing tooth surface wear, the classical Archard wear model is extensively applied. Khonsari and Masjedi [19] estimated the wear rate of spur gear by extending Archard theory to the mixed lubrication regime with fractional film defect. Wang et al. [20] studied the adhesive wear under mixed EHL by using modified Archard wear equation, and the effects of working parameters on the wear depth were investigated. Zhang et al. [21] predicted tooth wear rate in the mixed lubrication condition with the extended Archard theory. Although the gear surface wear has already been studied for some time, the coupling effect of contact performance has not been fully revealed yet, thus further investigations should be launched.

In the present work, an attempt is made to develop a comprehensive methodology to evaluate the effect of rolling-sliding and mild wear on contact performance. The gear contact is modeled with mixed lubrication and rolling-sliding process, while the surface topography is

updated by the oncoming and worn surfaces simultaneously. Based upon extracting stress cycles from the ordered instantaneous stress field, the relative fatigue life is evaluated by using the probabilistic fatigue model. Correlations between mild wear and surface contact fatigue is discussed with different surface finishing processes and wear coefficients.

## **2. Methodology**

### **2.1 Simulation of rolling-sliding contact**

For involute gear pair, the meshing process is characterized by five points, the engaging initiates at the start of active profile of the driving gear, then proceeds through the lowest point of single tooth contact (LPSTC) and the pitch point. The surface speed on driving gear is lower than driven gear in this stage, and the trend is opposite from the pitch point to HPSTC and recess point. The pure rolling only occurs at the pitch point, while in other area the motion is mixed rolling-sliding contact. Hence, a rolling-sliding contact frame is developed to simulate gear meshing process.

In the present work, the gear contact at a meshing point is represented by a cylinder pair according to gear meshing theory [22]. The work condition parameters such as load, speed and radius of curvature are assumed to be constant near the engagement point. The rolling-sliding contact procedure of a meshing cycle is defined as a loading passage. It is divided into 64 contact steps, in which the contact point moves through the target zone. As shown in Fig. 1, the simulation is performed during the period from outlet area entering the Target zone to inlet area exiting the Target zone. The variations of surface contact state and topography are documented in the Target zone. The calculation domain is  $-2 \leq x/b \leq 2$ ,  $-0.5 \leq y/l \leq 0.5$ , where  $b$  is the Hertzian contact half-width and  $l$  is the contact zone width. And the length of the Target zone is  $2b$ .

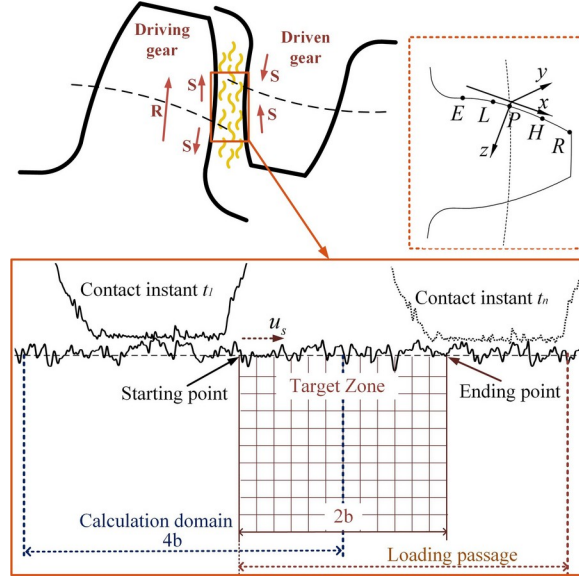


Fig. 1. Schematic diagram of the sliding-rolling contact.

The transient elasto-hydrodynamic lubrication procedure is performed at every contact instant. The contact pressure, film thickness and stress field are recorded. The surface topography is updated simultaneously for next contact moment from two aspects: the reduction of asperity height is calculated with mild wear equations, and the new surface roughness is engaged in terms of rolling-sliding speed. The surface roughness changes due to plastic deformation is assumed to be neglected under the rated torque condition [9]. At the end of one loading passage, the obtained stress history is combined with contact fatigue module to determine the fatigue life. Then the next loading passage can be repeated with the worn-in surface under cyclic load. This process could be repeated many times until the critical life or damage reached. The technical route of the model is illustrated in Fig. 2. In the following sections, the lubrication contact module and fatigue module will be described in detail.

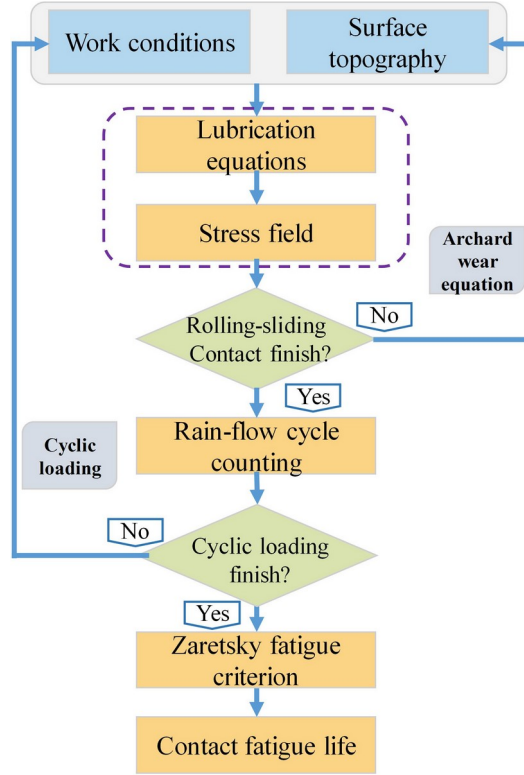


Fig. 2. Technical route of the contact fatigue model.

## 2.2 Transient lubrication contact model

The contact of rough surfaces under lubrication condition can be well modeled based on deterministic EHL theory [23]. At every contact instant, assuming the body forces are negligible, the fluctuation of pressure caused by the interaction between lubricant and asperities can be described by the generalized Reynolds equation [24]:

$$\frac{\partial}{\partial x} \left( \frac{\rho h^3}{12\eta} \frac{\partial p}{\partial x} \right) + \frac{\partial}{\partial y} \left( \frac{\rho h^3}{12\eta} \frac{\partial p}{\partial y} \right) = \frac{\partial(\rho u h)}{\partial x} + \frac{\partial(\rho h)}{\partial t} \quad (1)$$

Considering the non-Newtonian characteristic of lubricant, the rheological properties including density, viscosity and viscosity coefficient are given as:

$$\left\{ \begin{array}{l} \rho = \rho_0 (0.59 \times 10^9 + 1.34 p) / (0.59 \times 10^9 + p) \\ \eta = \eta_0 \exp \left[ (\ln \eta_0 + 9.67) \left[ (1 + 5.1 \times 10^{-9} p)^{z_e} - 1 \right] \right] \\ z_e = \alpha / [5.1 \times 10^{-9} (\ln \eta_0 + 9.67)] \\ \eta^* = \eta \left( \frac{\tau}{\tau_0} \right) / \sinh \left( \frac{\tau}{\tau_0} \right) \end{array} \right. \quad (2)$$

here, the viscosity  $\eta$  and density  $\rho$  are treated as functions of pressure. The ambit viscosity

and density are represented by  $\rho_0$  and  $\eta_0$ , respectively.  $z_e$  denotes the pressure–viscosity coefficient and  $\eta^e$  is the effective viscosity. The characteristic shear stress of lubricant is given as  $\tau_0=5\text{ MPa}$ .

Consuming the gap of mating surface is filled with lubricants, then the height of gap can be expressed by generalized film thickness equation:

$$h=h_0(t)+h_g+V_e(x,y,t)+S_c(x,y,t)+h_w(x,y,t)\quad(3)$$

The initial and geometry gap are denoted by  $h_0(t)$  and  $h_g$ , and  $V_e$  is the elastic deformation.  $S_c$  represents the composite time-varying surface topography.  $h_w$  is the variation of asperity height introduced by mild wear.

From the perspective of engineering evaluation, mild wear can be treated as classical Archard model since its low wear rate under a steady-state process. Considering the height of removed layer  $h_w=\Delta V/A_c$ , and the total load  $F_n$  also can be expressed as  $F_n=\bar{p}A_c$ , where  $A_c$  is the area of contact zone. Then the reduction of asperity height can be given as[25]:

$$h_w=k_l\frac{\bar{p}u_s t}{H_m}\quad(4)$$

where  $u_s$  denotes the sliding speed, and  $\bar{p}$  denotes the average contact pressure.  $t$  is the contact time on Surface 1, which can be represented by the length of contact zone as  $t=L_c/u_1$ .

Then the local wear height is:

$$h_w(x,y)=k_l\frac{p(x,y)L_c}{H_m}\left(\frac{u_s}{u_1}\right)\quad(5)$$

where  $H_m$  is the hardness of surface material, and  $k_l$  is wear coefficient. To simplify the application, the wear coefficient is give as a constant according to the published works [13]. The roughness profile is updated every  $\Delta N$  numbers of contact cycles based on “jump-in-cycle” method [26]. The contact conditions and wear rate are assumed to stay the same in a fixed loading block. In this work the interval of loading block is given as  $\Delta N=1.0\times 10^6$  for compromise between calculation time and perdition precision.

### 2.3 Stress history and contact fatigue criterion

The transient pressure and traction can be obtained by solving the above govern equations of

lubricant, then the subsurface stress field is efficiently calculated by using the DC-FFT method:

$$\sigma_{ij} = IFFT(C_{ij}^p(x-k, y-l)\tilde{p}(k, l) + C_{ij}^q(x-k, y-l)\tilde{q}(k, l)) \quad (6)$$

where  $\tilde{p}$  and  $\tilde{q}$  are pressure and traction after zero padding and transforming to frequency domain.  $IFFT$  denotes inverse fast Fourier transform.  $C_{ij}^p$  and  $C_{ij}^q$  are pressure-stress influence coefficients derived via Green functions [27].

The variation of stress field due to the mixed rolling-sliding motion can be described by the time series of stress. The instantaneous field is arranged in terms of the discretized time-steps then the stress history can be obtained. The rain-flow counting method can be applied to extract the cycles contained in the stress history based on the stress-strain hysteresis loops. The detail characteristics of stress cycles would be presented in Section 3.1.

Probabilistic contact fatigue model is extensively applied in engineering to evaluate contact fatigue life. Many related efforts have been made since the pioneering work of Lundberg and Palmgren [28]. Based on the ideal of Weibull statistical strength theory, probabilistic contact fatigue model was continuously developed by Ioannides and Harris [29], Tallian [30], Zaretsky [31], etc. The presented work aims to evaluate the surface contact fatigue related to near surface stress concentration, in which the influence along depth direction is eliminated. Zaretsky model is adaptive since the fatigue life calculation is independent on the depth term [32]. Herein, to investigate the effect of rolling-sliding contact, Zaretsky's equation is applied in the perspective of relative contact fatigue life. The model is given as:

$$\ln \frac{1}{S} = AN^e \int_V (\tau_e)^{ec} dV \quad (7)$$

where  $S$  is the probability of survival, and  $\tau_e$  is the equivalent stress.  $A, e, c$  are material fatigue parameters involved with the Weibull slope and the stress exponent. According to the gear contact fatigue tests conducted by Zhu et al. [4], it can be given as  $e=1.1, c=4.5$ . The fatigue life of rolling-sliding contact ( $N_{\text{rs}}$ ) and pure rolling ( $N_{\text{pr}}$ ) can be represented as:



$$(N_{rs})^e = \frac{\ln 1/S}{A \int_V (\tau_e^i)^{ec} dV} \quad (8)$$

$$(N_{pr})^e = \frac{\ln 1/S}{A \int_V (\tau_e^r)^{ec} dV} \quad (9)$$

Consider the stress cycles in rolling-sliding contact, the relative contact life is expressed as

$$L_r = \frac{N_{rs}}{N_{pr}} = \left[ \frac{\Delta V \cdot (\tau_e^r)^{ec}}{\sum_{i=1}^k \Delta V \cdot (\tau_e^i)^{ec}} \right]^{-1/e} = \left[ \sum_{i=1}^k (\tau_e^i / \tau_e^r)^{ec} \right]^{1/e} \quad (10)$$

### 3. Results and discussion

The discussed gear pair parameters, as list in Table 1, come from a 2MW wind turbine, in which the driven gear (pinion) of intermediate parallel stage experienced frequent failures in engineering practice. Herein, the following analysis mainly focus on the HPSTC of pinion, which experiences Hertzian pressure of 1.2 *GPa* under the rated input torque. Under the rated conditions, the rolling speed and slid-to-roll ratio are 3.4 *m/s* and  $-0.3$ , respectively. The surface topography is measured from generating grinding tooth by an optical profiler with high resolution (InfiniteFocus, Alicona, Graz, Austria). The processing and sampling of measured topography data can be referred in Ref. [33]. Fig. 3a-b present the roughness profiles in the mid-plane (x-o-z cross section,  $y=0$ ) of Surface 1 and 2, respectively. Two surfaces move at speed of  $u_1$  and  $u_2$ , which takes a time-varying composite surface topography into the Target zone. The corresponding rough contact results of the presented roughness are compared with smooth contact case in Fig. 4. It should be noticed that although the simulation is based on three-dimensional line contact EHL, just the pressure and stress on the mid-plane ( $y=0$ ) are presented for simplification. The distributions of instantaneous pressure and film thickness are shown in Fig. 4a. The pressure spikes reach up to 2.5–3 *GPa*, which are 2–3 times higher than the maximum pressure of smooth contact. The variation of pressure peaks introduced by the interaction asperities and lubricants have been widely discussed in the studies about mixed EHL [23] and micro EHL [6]. By

comparing with related results, one can draw a conclusion with certainty that the rough surface contact would lead to drastic pressure spikes and weak lubricant film. This point has to be emphasized because it is one of the most important inducements for many common types of contact failure, such as micropitting, spalling and scuffing, etc. And it is also the direct stimulus of stress fluctuations at or very near mating surface. It can be readily to see from the distribution of shear stress  $\tau_{xz}$  in Fig. 4b, these pressure peaks cause severe stress concentration at sub-surface, comparing with the smooth case.

Table 1 Gear and lubricant parameters

Parameters	Values
Number of teeth	$Z_1=121, Z_2=24$
Normal module	$m_0=0.011\text{ m}$
Face width	$b_w=0.295\text{ m}$
Pressure Angle	$\alpha_0=20^\circ$
Poisson's ratio	$\nu=0.3$
Elastic modules	$E=210\text{ GPa}$
Gear shifting coefficients	$x_1=0.0034, x_2=0.4$
Rated input torque	$T_1=282768\text{ Nm}$
Input speed	$N_1=154\text{ r/min}$
Ambient density	$\rho_0=870\text{ kg/m}^3$
Ambient dynamic viscosity	$\eta_0=0.08\text{ pa}\cdot\text{s}$
Viscosity-pressure coefficient	$\alpha=2.1 \times 10^{-8}\text{ pa}^{-1}$
Kinematic viscosity at 40°C	$220\text{ mm}^2/\text{s}$
Kinematic viscosity at 100°C	$28.5\text{ mm}^2/\text{s}$

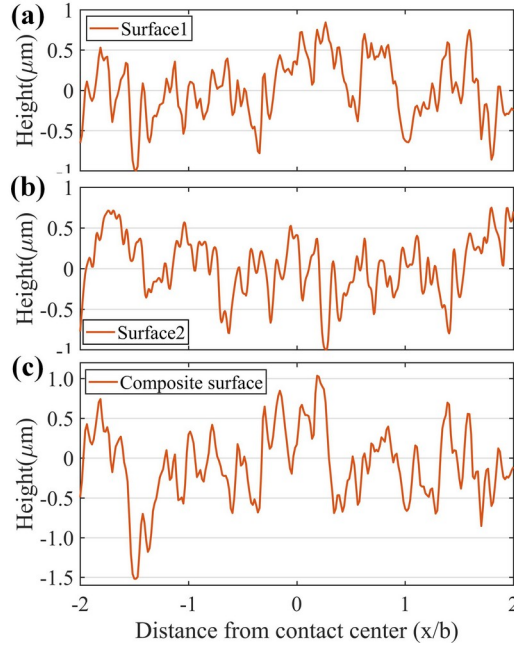


Fig. 3. Roughness profiles in the x-o-z section at  $y=0$ ,  
(a) Surface1, (b) Surface2, (c) Composite Surface.

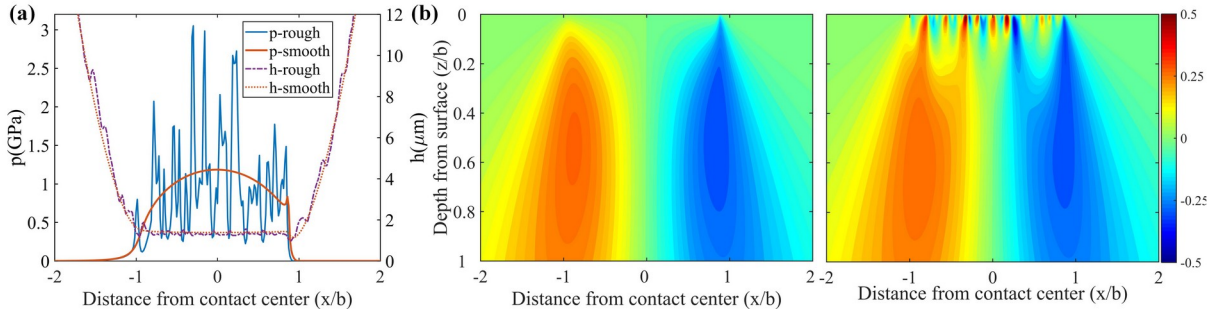


Fig. 4. The distribution of (a) pressure and film thickness,  
(b) shear stress  $\tau_{xz}$  under and smooth contact.

### 3.1 Instantaneous pressure and stress history

Fig. 5 presents the instantaneous pressure at three contact moments. It should be noticed that the following discussion only focuses on the contact conditions in the Target zone. The entire loading period could be treated as the contact zone moves through the Target zone. At the instant of  $t=0.25T$  and  $t=0.75T$ , part of the contact area is outside the Target zone. At the instant of  $t=0.5T$ , the contact center is overlaps with the center of Target zone.

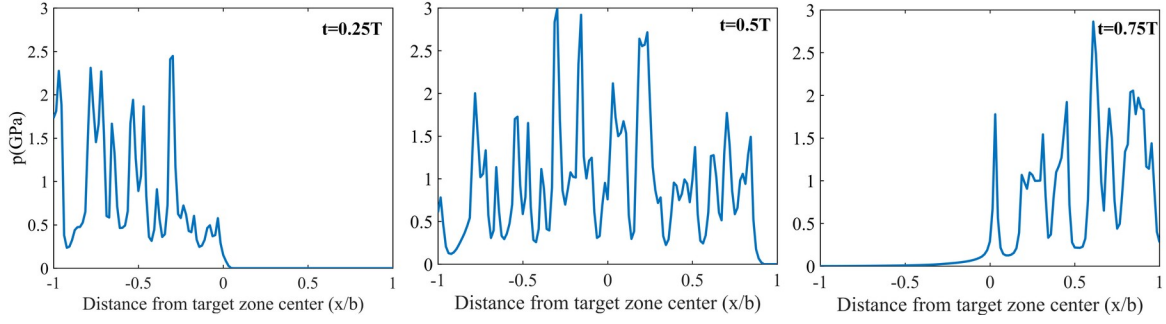


Fig. 5. The distributions of pressure and film thickness at different contact instants.

And the corresponding stress field are shown in Fig. 6 a1-c1, respectively. The severe zones of stress concentration exhibit within the depth about  $0.1b$ , which is the characteristic location of surface cracks for micropitting. These instantaneous distributions of pressure and stress coincide with the typical results of mixed EHL analysis. However, it is necessary to consider the stress history of the entire loading period for an accurate contact fatigue analysis, especially for rough contact. Fig. 6a2-c2 show the stress history of the center of Target zone. It may be noted that, for a given material point, the maximum stress may not occur at the contact instant. Specifically, the highest stress experienced by the center of Target zone is not observed at the moment of  $t=0.5T$ , indicating that the instantaneous stress may not enough for evaluating the fatigue performance. It can be seen that several stress peaks occur for  $\tau_{xz}$  and at least two peaks for  $\sigma_{zz}$  during  $t=0.25T-0.75T$ . Fig. 7 further depicts the extracted stress history of  $\tau_{xz}$  at the depth of  $z=0.03b$ . Four stress cycles are marked with red dash line by using rain-flow counting method. It can be readily to see that the material point experiences four micro-cycles in one contact passage. The sub-cycles included in the stress history is described as stress micro-cycles, which is of significant influence on the contact fatigue performance. To evaluating the overall properties of stress field and micro-cycles, octahedral shear stress is selected as the equivalent stress in next sections.

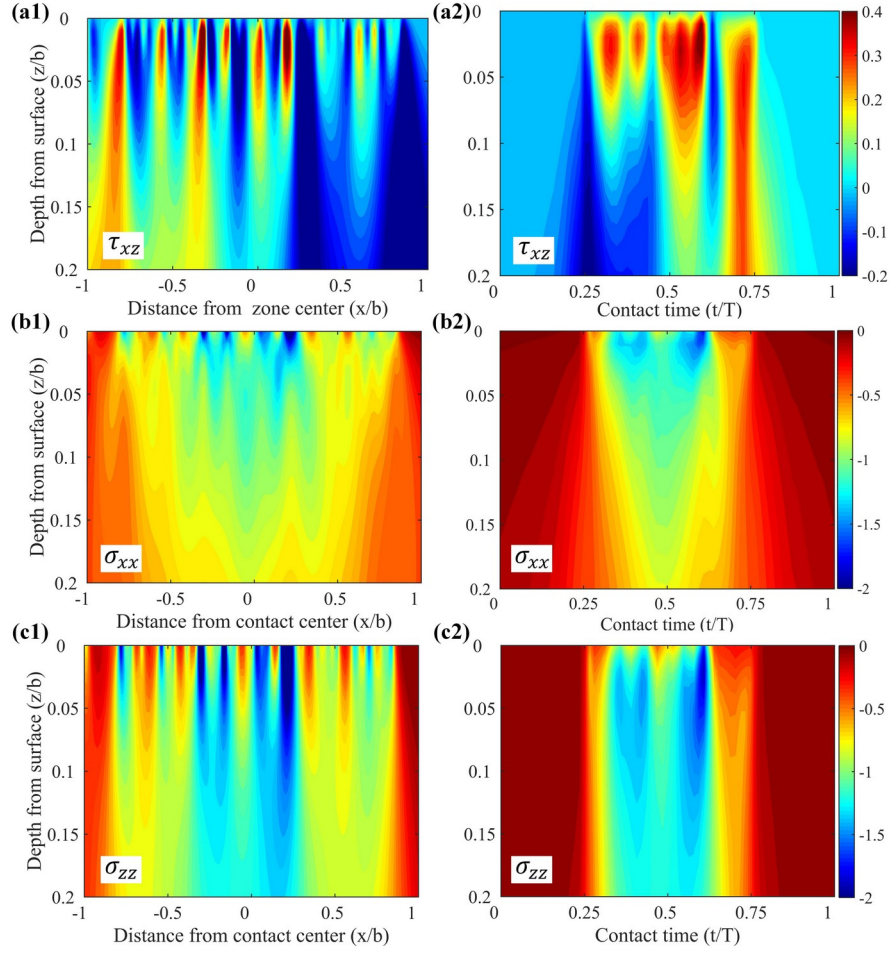


Fig. 6. (a1)-(c1) The transient distributions of stress components  $\tau_{xz}$ ,  $\sigma_{xx}$ ,  $\sigma_{zz}$ ; (a2)-(c2) stress histories of stress components  $\tau_{xz}$ ,  $\sigma_{xx}$ ,  $\sigma_{zz}$ .

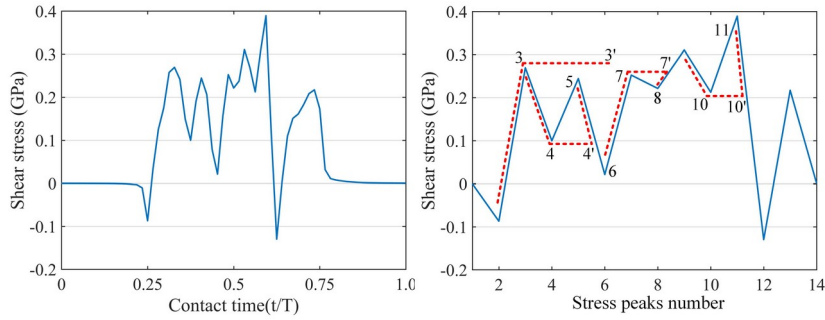


Fig. 7. Schematic diagram of rain-flow cycles counting method.

### 3.2 Stress micro-cycles in rolling-sliding contact

In this section, the stress histories of different rolling-sliding contacts are investigated by changing the slid-to-roll ratio, while maintaining a constant pressure. Fig. 8 presents the contour plots of stress history in the Target zone for three different rolling-sliding contact

type: negative sliding, pure rolling and positive sliding. The dark red patches indicate the high stress area caused by the interaction of asperities in the contacting surface. These gapped bands or patches exhibit obvious trajectories of stress spikes, which reflect the relative movement of surface asperities. The stress history distribution shows great difference from pure rolling to rolling-sliding contact. For pure rolling contact, the high stress area is continuous ridge-like band, which implies the relatively static state of two surface. While for rolling-sliding contact, the scattered patches represent the relative sliding of asperities. The surface of Target zone meets different roughness at every contact instant due to the sliding motion. As another evidence for the sliding motion, two traces of stress spikes can be found in both negative and positive sliding contact. For negative and positive sliding, the inclined traces of spikes point to different directions. In general, stress spikes introduced by asperities on both Target zone surface (Surface 1) and counter-surface (Surface 2) can be identified based on direction of traces.

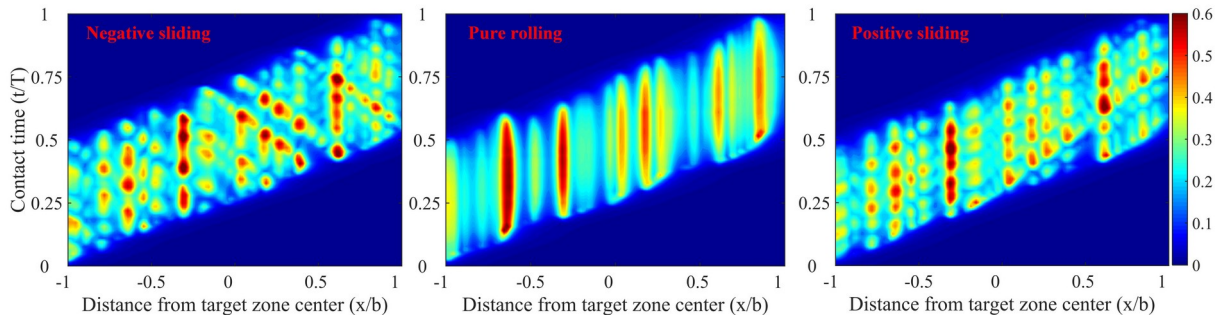


Fig. 8. Stress history of different rolling-sliding contact in the Target zone.

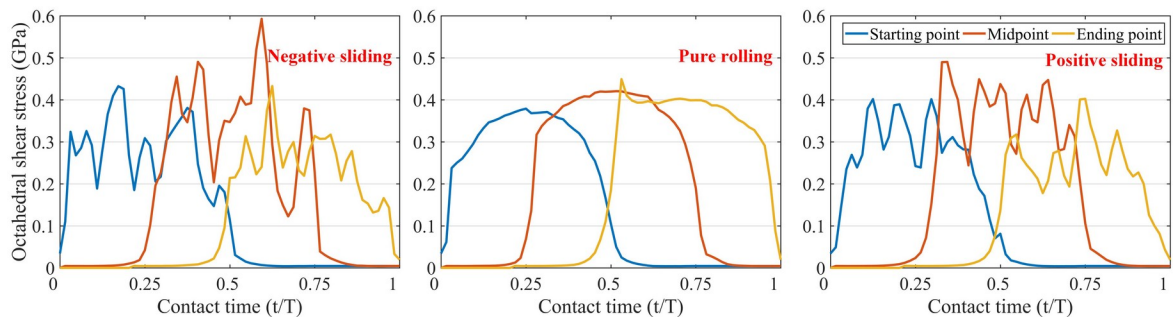


Fig. 9. Stress-time section plots at different position.

Fig. 9 further shows the cross section of time-stress plot at different positions of the Target zone. These stress profiles clearly illustrate the difference of stress micro-cycles between rolling-sliding and pure rolling contact. The stress history of rolling-sliding contact could

contain several stress micro-cycles. From the view of fatigue damage accumulation, the material points in rolling-sliding contact could take more damage. Besides, the maximum stress in rolling-sliding contact is obviously higher than pure rolling case.

Fig.10 presents the overall effect of stress micro-cycles on contact fatigue. Fig. 10a-b show the equivalent stress range of all the micro-cycles in the Target zone. The red curve denotes the maximum stress of pure rolling contact, in which the stress history is treated as one full cycle. The maximum equivalent stress of pure rolling is  $0.54\text{ GPa}$  at  $x=-0.59b$ . While the maximum range of stress micro-cycles is  $0.69\text{ GPa}$  and  $0.67\text{ GPa}$  at  $x=-0.3b$  for negative and positive rolling-sliding contact, respectively. Because kinematic sliding takes more roughness, which might involve the higher or lower asperities, into contact in one loading passage.

Fig. 10c illustrates the relative contact fatigue life compared with pure rolling. The fatigue life of rolling-sliding contact is obviously lower than pure rolling case. The mean value of relative fatigue life is 0.205 and 0.215 for negative and positive sliding, respectively. The possible reason for the minor difference is that the number of high stress cycle for both cases is close. However, in practice, more fatigue damage usually reported in the negative sliding area of gears. This is due to the criterion applied here is for fatigue life of crack initial, while the other influence, such as crack propagation, is neglected. In the area  $-0.4b \leq x \leq 0$ , marked by black box, the relative life is noticeable lower than the average. Compared with the same position in equivalent stress range plots, a larger number of stress micro-cycles with higher amplitude can be found. In the case of negative sliding, the relative life as high as 0.39 is found at  $x=-0.59b$ , whereas for positive sliding the lower life, 0.323, is observed. Fig. 10d lists the stress ranges of two contact positions. If all the cycles are considered, seven and ten stress micro-cycles can be found at  $x=-0.59b$  and  $x=-0.14b$ , respectively. For the position of  $x=-0.59b$ , two cases show similar range of stress cycles except the first one. The amplitudes of the first micro-cycles are  $0.113\text{ GPa}$  and  $0.051\text{ GPa}$  for negative and positive sliding, respectively. This fact suggests that the computing of fatigue life is sensitive to the stress range and the stress cycles, which needs to be discreet for gear fatigue application. To sum up, the relative fatigue life not only depends on amplitude, but amount of stress micro-



cycles.

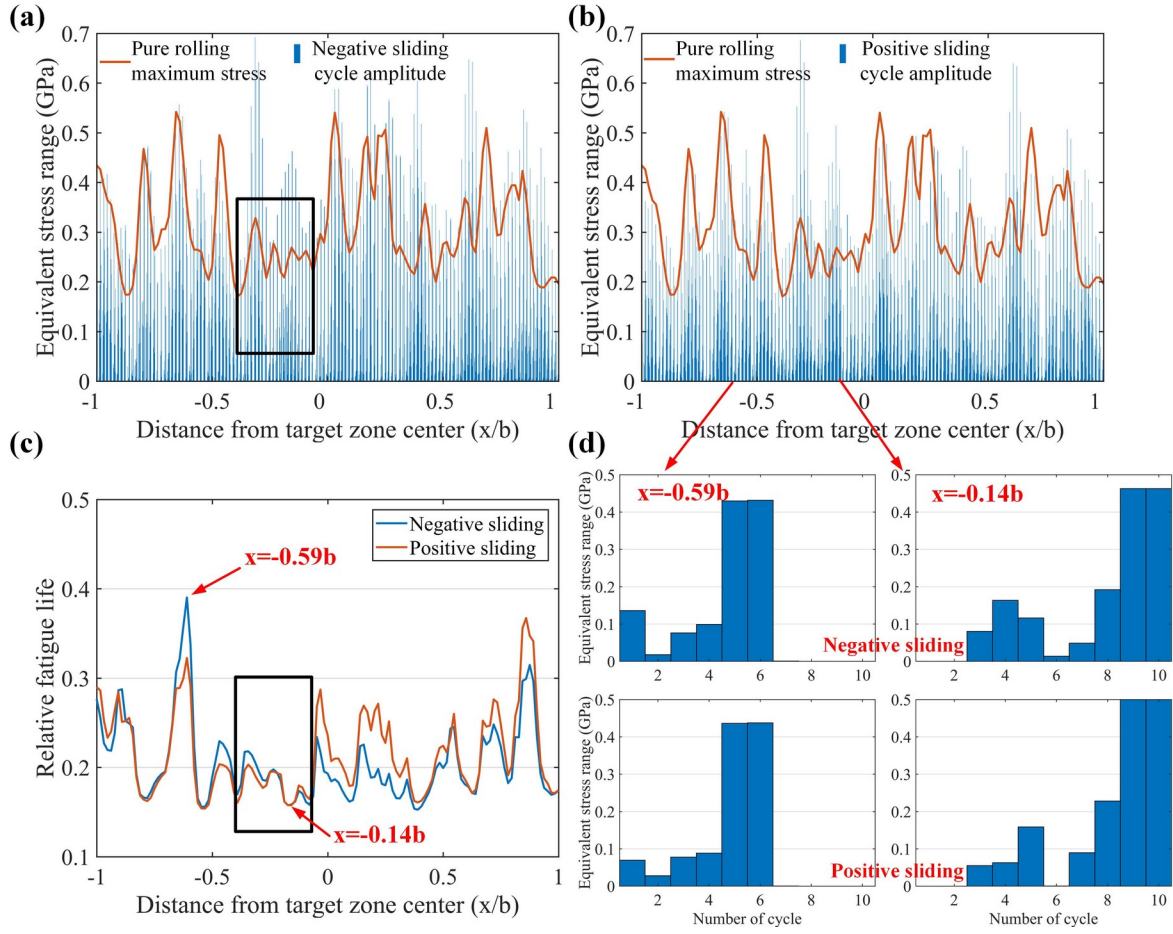


Fig. 10. The effects of rolling-sliding contact on stress micro-cycles and relative fatigue life,

(a) stress cycle amplitude of negative sliding, (b) positive sliding,

(c) relative fatigue life, (d) stress cycles at specific position.

### 3.3 The effect of wear-in under cyclic loading

The evolution of gear contact performance is mainly reflected in the variation of surface topography and deterioration of local material properties. To investigate the evolution of roughness and its effects on contact performance, the cyclic loading is applied on the developed contact model based on the “jump-in-cycle” method. The simulation is carried out

with three different wear coefficients:  $k_l = 1.0 \times 10^{-11} [s]$ ,  $k_l = 0.5 \times 10^{-11} [s]$  and

$k_l = 0.25 \times 10^{-11} [s]$ . Fig. 11 depicts the variation of surface topography and pressure during the



first 10 million (M) cycles for the case of  $k_l=1.0 \times 10^{-11} [s]$ . Fig. 11a-b show the height of asperities continuously reduce due to surface pressure and kinematic sliding. The protruding parts have suffered more wear since the higher contact pressure, as presented by Point b and d. However, the change is relatively small for the valleys, such as Point a and c. Fig. 11c-d show the surface pressure at the instant of  $t=0.5T$ . The pressure spikes are impaired due to the decreasing asperity heights. The pressure at Point b reduces from  $2.79 GPa$  to  $1.77 GPa$ , and for Point d is  $2.15 GPa$  to  $1.67 GPa$ . It worth noticed that the decreasing rate for the first 5M cycles higher than the last 5M cycles. Specifically, for Point d the pressure peak declines 14.16% from 1M to 5M cycles, while it declines 7.69% from 6M to 10M cycles. The variation of pressure after 5M and 10M cycles is agree well with the analysis results of Kadiric et al. [34]. However, the pressure valleys, such as Point c and d, show a little increase. It should be noticed that the pressure spikes are not consistently one-to-one corresponded with the peak of asperities. The main reason is that the contour-surface (Surface 2) would affect the time-varying composite roughness. The higher pressure leads to the sharp reduction of asperities height, while the worn roughness takes mitigated pressure distribution. The coupling relation between roughness and pressure lead to the evolution of contact performance.

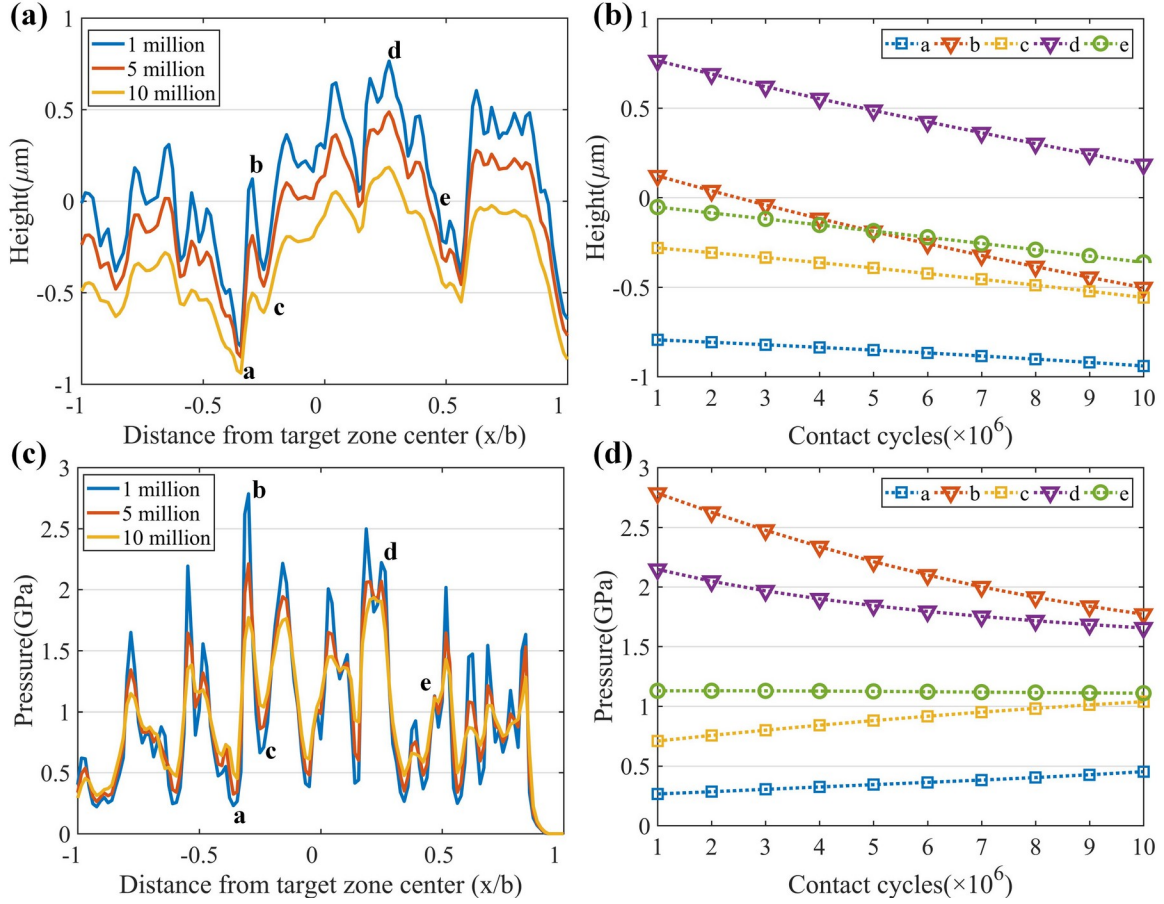


Fig. 11. The effects of mild wear on (a)-(b) surface roughness and (c)-(d) pressure.

Fig. 12a shows the change of stress history from 1M to 10M cycles. It can be seen that the stress spikes represented by dark red patches gradually weakened, and the trajectories of stress almost invisible. The maximum stress reduces from  $0.67\text{ GPa}$  to  $0.45\text{ GPa}$  after 10M cycles. Fig. 12b presents frequency histogram of the stress micro-cycles. The micro-cycles with amplitude less than  $0.1\text{ GPa}$  accounted for more than 50%. However, the micro-cycles with the higher amplitude are the main contributor for the lower fatigue life. The rate of these micro-cycles greatly reduces after 10M cycles, which means the stress concentration is significantly mitigated since the decreasing of asperity height.

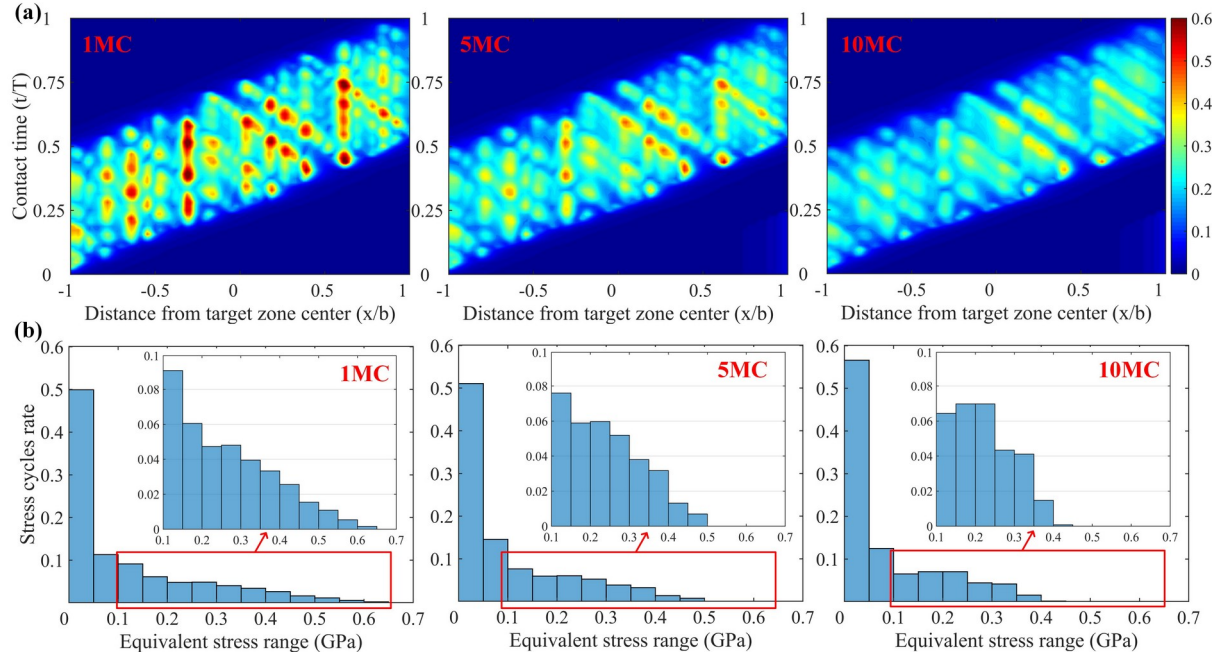


Fig. 12. The effects of mild wear on stress micro-cycles, (a) stress histories, (b) frequency histogram of the stress micro-cycles.

The variations of surface roughness and relative contact fatigue life under different wear coefficients are shown in Fig.13. The relative fatigue life gradually declines as the loading cycle increases. The decreasing roughness causes the increase of relative life, since the reduced pressure peak and impaired stress concentration. The higher wear coefficient leads to more asperity removal and higher relative fatigue life. The results above support the correlation between surface contact fatigue and mild wear. In general, mild wear tends to smooth the surface then decrease the risk of surface creak initiation. This is in line with existing results reported by Liu et al. [16]. However, the accumulation of fatigue damage usually impairs contact performance under cyclic loading. This suggest that the coupling influence of the material deterioration caused by fatigue damage need to be considered for more precise simulation.

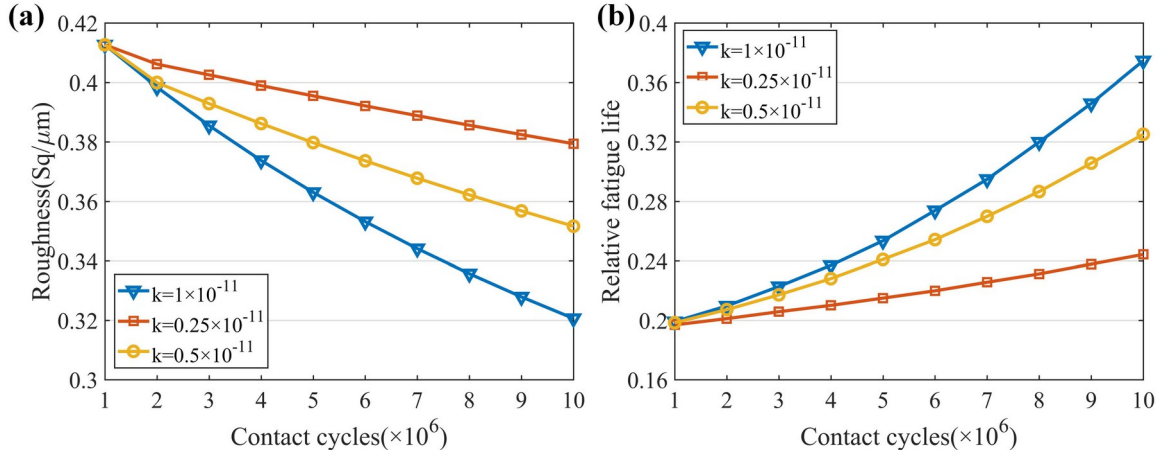


Fig. 13. The effects of mild wear on (a) surface roughness and (b) relative fatigue life under different wear coefficients.

### 3.4 The effect of surface finishing

To investigate the effect of surface finishing on contact performance, two different types of surface topography, namely superfinishing (SF) and grinding coating (GC) are applied in the simulation. The surfaces are assumed to have lower wear coefficient ( $k_l=0.5 \times 10^{-11} [s]$ ) due to the different surface finishing processes. The evolution of roughness profiles is shown in Fig. 14(a)-(b). The SF surface obviously declines whereas the change of the GC surface is relatively small. It is no doubt that lower wear coefficient leads to less reduction of asperity. However, the roughness amplitude is another reason for the lower wear rate of GC surface. The same wear volume would significantly change the SF surface since its lower roughness amplitude. Fig. 14 (c)-(d) present the corresponding pressure profiles during the 10M cycles. The intensive asperities of SF surface cause more pressure spikes, while the pressure distribution of the GC surface is similar to the discussed one above. With the increasing wear volume, the pressure profile of SF surface gets close to Hertzian pressure, whereas the change of GC surface is limited.

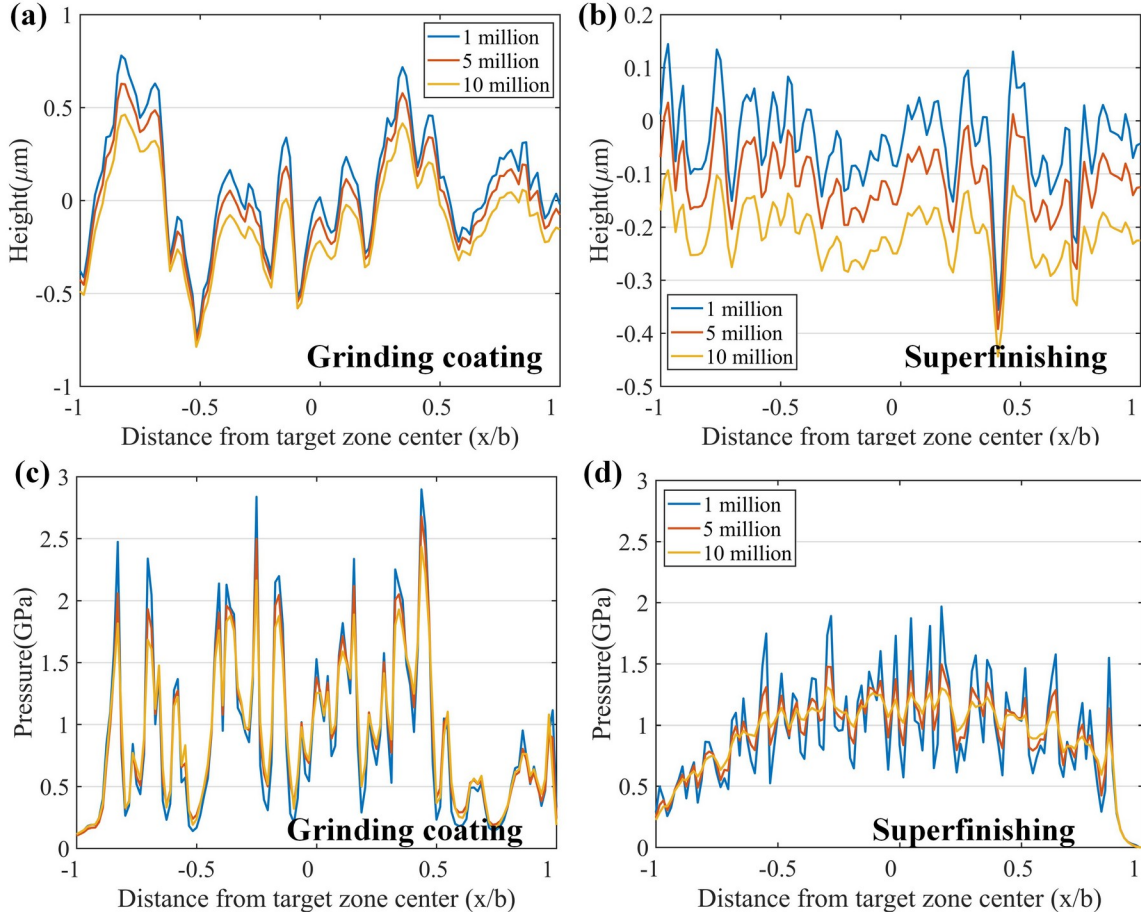


Fig. 14. The variation of roughness profiles with (a) grinding coating surface, (b) superfinishing surface, the variation of pressure with (c) grinding coating surface, (d) superfinishing surface.

The stress histories in Fig. 15 illustrates the similar trend to the variation of pressure. For GC surface the trajectories of stress spikes is clearly visible after 10M cycles. For SF surface it is unclear even after 5M cycles. Fig. 16 show the variation of relative fatigue life and roughness of two surfaces. The roughness ( $S_q$ ) of GC surface decreases from  $0.323$  to  $0.277 \mu\text{m}$ , and SF surface decreases from  $0.095$  to  $0.053 \mu\text{m}$ , which drops more than 44% during 10M cycles. As the decreasing roughness, the relative fatigue life of SF surface increases steeply. It can be seen that the evolution of surface roughness has a significant influence on the relative life. The change of roughness and relative life suggest that SF surface has better wear-in performance.

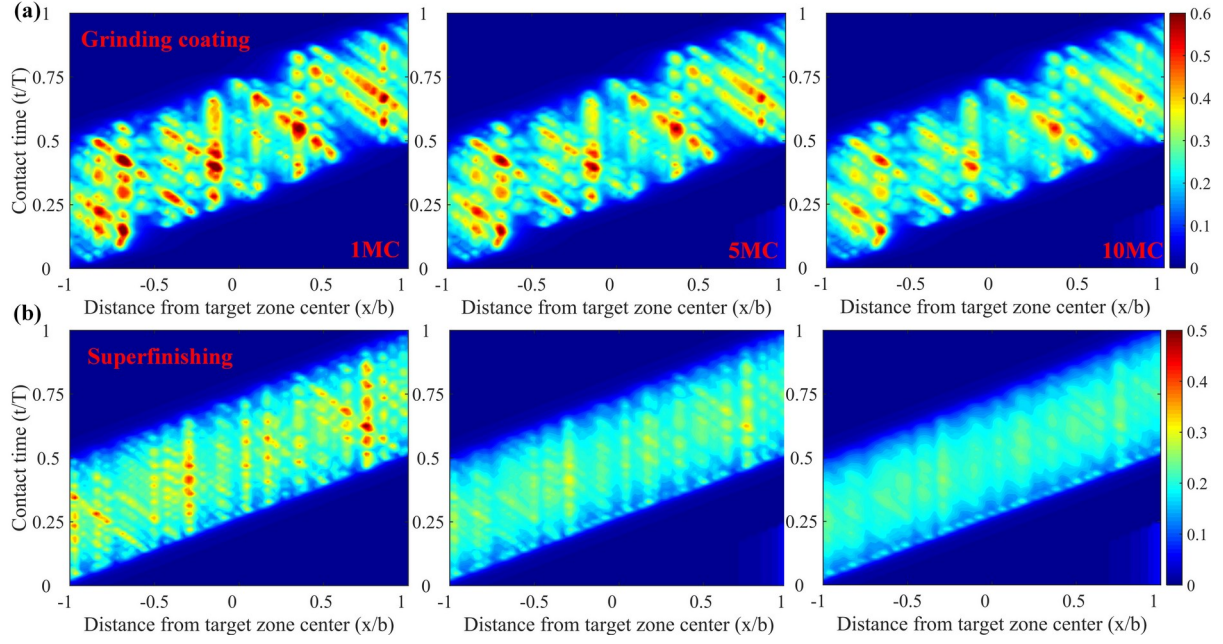


Fig. 15. The variation of stress history with (a) grinding coating surface, (b) superfinishing surface.

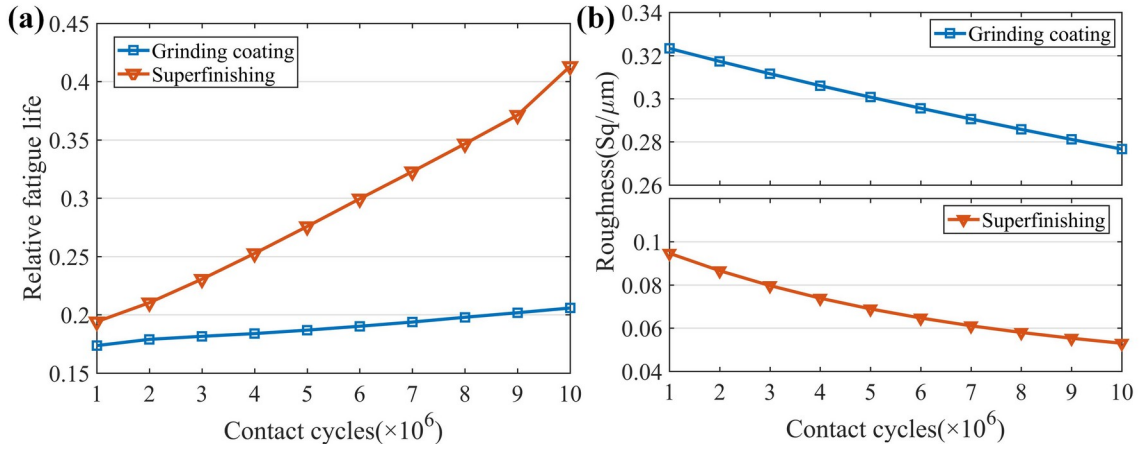


Fig. 16. The variation of (a) relative fatigue life and (b) roughness with different surfaces.

## 5. Conclusion

This paper presented a comprehensive contact fatigue model, which works well to capture the effects of rolling-sliding and mild wear on contact performance. The instantaneous pressure and stress field is calculated with the transient mixed EHL process. Rolling-sliding contact is simulated with the time-varying roughness topography updated by mild wear. Then the stress cycles are extracted and the relative contact fatigue life is obtained by Zaretsky criterion. With the developed framework, the influences of different wear coefficients and finishing surfaces were studied. Conclusions can be summarized as follows.



1. For rolling-sliding contact of rough surfaces, material points at or near surface experience more than one stress cycle. As contact area traverses a fixed zone, the drastic stress fluctuation could introduce many micro-cycles related to the time-varying stress field. To accurately evaluate gear surface contact fatigue, it should not only consider the transient mixed EHL condition, but it is necessary to consider the stress history introduced by the rolling-sliding contact of rough surface during a loading cycle.
2. Comparing with pure rolling, the contact fatigue life is obviously lower in rolling-sliding contact. In the studied cases, the mean values of relative life are as lower as 0.205 and 0.215 for negative and positive sliding, respectively. The increases in the number and amplitude of stress micro-cycles is found to be the main contributors to the reduction of fatigue life.
3. The variation of surface topography resulting from mild wear is of great influence on the evolution of contact performance. Mild wear tends to smooth the surface, subsequently mitigates the stress concentration and reduces stress micro-cycles, then decrease the risk of surface contact fatigue.
4. Surface superfinishing could effectively reduce stress micro-cycles and increase contact fatigue life. The roughness ( $S_q$ ) of grinding coating surface decreases from 0.323 to 0.277  $\mu m$ , and superfinishing surface decreases from 0.095 to 0.053  $\mu m$ , during the simulated 10 million cycles. The better wear-in performance is found in superfinishing compared with grinding coating surface.

#### **Authorship contribution statement**

Ye Zhou: Conceptualization, Methodology, Writing - original draft. Caichao Zhu: Supervision, Project administration, Funding acquisition. Huaiju Liu: Conceptualization, Writing - review & editing. Houyi Bai: Formal analysis, Writing - review & editing. Xiaona Xu: Investigation, Writing - review & editing.

#### **Acknowledgement**

This project is supported by National Natural Science Foundation of China (Grant No. 52005057), and the Natural Science Foundation of Chongqing, China (Grant No. cstc2020jcyj-msxmX0643), and the Fundamental Research Funds for the Central Universities

(Grant No. 2020CDJQY-A069).

## Nomenclature

$b$	Half Hertzian contact width ( $m$ )
$e, c$	Material fatigue parameters relating to Weibull slope
$C_{ij}^p, C_{ij}^q$	Force-stress influence coefficient
$D_s$	Sliding distance ( $m$ )
$F_n$	Total applied load ( $N$ )
$h$	Film thickness ( $m$ )
$h_0$	Gap height between surfaces ( $m$ )
$h_g$	Geometry gap between surfaces ( $m$ )
$H_m$	Material hardness ( $Pa$ )
$k_l$	Wear coefficient of lubrication contact
$L_c$	Contact length ( $m$ )
$L_r$	Relative contact fatigue life
$N$	Fatigue life cycle
$p$	Surface pressure ( $Pa$ )
$p_H$	Hertzian maximum pressure ( $Pa$ )
$q$	Shear traction ( $Pa$ )
$S$	Probability of survival
$S_c$	Composite surface roughness ( $m$ )
$t$	Time ( $s$ )
$u_s$	Sliding velocity ( $m/s$ )
$u_r$	Rolling velocity ( $m/s$ )
$V_e$	Elastic deformation ( $m$ )
$x, y, z$	Coordinates ( $x$ is parallel to rolling direction)
$\alpha$	Pressure–viscosity coefficient
$\eta$	Viscosity of the lubricant ( $Pa \cdot s$ )
$\eta_0$	Ambient viscosity of the lubricant ( $Pa \cdot s$ )
$\eta^i$	Equivalent viscosity of the Eyring fluid ( $Pa \cdot s$ )



$\rho$	Current density of the fluid ( $kg/m^3$ )
$\rho_0$	Ambient density of the lubricant ( $kg/m^3$ )
$\Delta N$	The number of cycle interval $\dot{\epsilon}$
$\Delta h_w$	Wear depth ( $m$ )
$\tau$	Film shear stress ( $Pa$ )
$\tau_0$	Eyring characteristic shear stress ( $Pa$ )
$\tau_e$	Equivalent shear stress ( $Pa$ )
$IFFT$	Inverse Fourier transform $\dot{\epsilon}$

## References

- [1] Sheng S. Wind turbine micropitting workshop: a recap. National Renewable Energy Laboratory (NREL), Golden, CO.; 2010.
- [2] Norway AIB. Report on the air accident near Turøy, Øygarden municipality, Hordaland county, Norway 29 April 2016 with Airbus Helicopters EC 225 LP, LN-OJF. Lillestrøm, Norway 2018.
- [3] Liu H, Liu H, Zhu C, Parker RG. Effects of lubrication on gear performance: A review. Mechanism and Machine Theory. 2020;145:103701.
- [4] Zhu D, Ren N, Wang QJ. Pitting Life Prediction Based on a 3D Line Contact Mixed EHL Analysis and Subsurface von Mises Stress Calculation. Journal of Tribology. 2009;131:041501.
- [5] Li S, Kahraman A, Klein M. A fatigue model for spur gear contacts operating under mixed elastohydrodynamic lubrication conditions. Journal of Mechanical Design. 2012;134:041007.
- [6] Evans HP, Snidle RW, Sharif KJ, Shaw BA, Zhang J. Analysis of Micro-Elastohydrodynamic Lubrication and Prediction of Surface Fatigue Damage in Micropitting Tests on Helical Gears. Journal of Tribology. 2012;135.
- [7] Li S, Anisetti A. A tribo-dynamic contact fatigue model for spur gear pairs. International Journal of Fatigue. 2017;98:81-91.
- [8] Zhou Y, Zhu C, Gould B, Demas NG, Liu H, Greco AC. The effect of contact severity on micropitting: simulation and experiments. Tribology International. 2019;138:463-72.
- [9] Zhou Y, Zhu C, Liu H, Song H. Investigation of Contact Performance of Case-Hardened Gears Under Plasto-elastohydrodynamic Lubrication. Tribology Letters. 2019;67:92.
- [10] Wang W, Liu H, Zhu C, Wei P, Wu W. Micromechanical analysis of gear fatigue-ratcheting damage considering the phase state and inclusion. Tribology International. 2019;136:182-95.
- [11] Lainé E, Olver AV, Beveridge TA. Effect of lubricants on micropitting and wear. Tribology International. 2008;41:1049-55.
- [12] Brandao JA, Martins R, Seabra JH, Castro MJ. Surface damage prediction during an FZG gear micropitting test. Proceedings of the Institution of Mechanical Engineers, Part J: Journal of Engineering Tribology. 2012;226:1051-73.
- [13] Morales-Espejel GE, Rycerz P, Kadiric A. Prediction of micropitting damage in gear teeth contacts considering the concurrent effects of surface fatigue and mild wear. Wear. 2018;398-399:99-115.

- [14] Morales-Espejel GE, Brizmer V. Micropitting modelling in rolling–sliding contacts: application to rolling bearings. *Tribology Transactions*. 2011;54:625-43.
- [15] Guilbault R, Lalonde S. A stochastic prediction of roughness evolution in dynamic contact modelling applied to gear mild wear and contact fatigue. *Tribology International*. 2019;140:105854.
- [16] Liu H, Liu H, Zhu C, Tang J. Study on gear contact fatigue failure competition mechanism considering tooth wear evolution. *Tribology International*. 2020:106277.
- [17] Pu W, Zhu D, Wang J, Jane Wang Q. Rolling–sliding contact fatigue of surfaces with sinusoidal roughness. *International Journal of Fatigue*. 2016;90:57-68.
- [18] Zhou Y, Zhu C, Liu H. A micropitting study considering rough sliding and mild wear. *Coatings*. 2019;9:639.
- [19] Masjedi M, Khonsari M. On the prediction of steady-state wear rate in spur gears. *Wear*. 2015;342:234-43.
- [20] Wang H, Zhou C, Lei Y, Liu Z. An adhesive wear model for helical gears in line-contact mixed elastohydrodynamic lubrication. *Wear*. 2019;426-427:896-909.
- [21] Zhang J-g, Liu S-j, Fang T. On the prediction of friction coefficient and wear in spiral bevel gears with mixed TEHL. *Tribology International*. 2017;115:535-45.
- [22] Liang C, Song C, Zhu C, Wang Y, Liu S, Sun R. Investigation of Tool Errors and Their Influences on Tooth Surface Topography for Face-Hobbed Hypoid Gears. *Journal of Mechanical Design*. 2020;142.
- [23] Zhu D, Wang QJ. Elastohydrodynamic lubrication: a gateway to interfacial mechanics—review and prospect. *Journal of Tribology*. 2011;133:041001.
- [24] Hu Y-Z, Zhu D. A full numerical solution to the mixed lubrication in point contacts. *Journal of Tribology*. 2000;122:1-9.
- [25] Archard J. Contact and rubbing of flat surfaces. *Journal of applied physics*. 1953;24:981-8.
- [26] Warhadpande A, Sadeghi F, Kotzalas MN, Doll G. Effects of plasticity on subsurface initiated spalling in rolling contact fatigue. *International Journal of Fatigue*. 2012;36:80-95.
- [27] Liu S, Wang Q. Studying Contact Stress Fields Caused by Surface Traction With a Discrete Convolution and Fast Fourier Transform Algorithm. *Journal of Tribology*. 2002;124:36.
- [28] Lundberg G, Palmgren A. Dynamic Capacity of Rolling Bearings. *Journal of Applied Mechanics*. 1949;16:165-72.
- [29] Ioannides E, Harris TA. A new fatigue life model for rolling bearings. *Journal of Tribology*. 1985;107:367-78.
- [30] Tallian T. Simplified contact fatigue life prediction model—Part II: New model. *Journal of Tribology*. 1992;114:207-13.
- [31] Zaretsky EV. Fatigue criterion to system design, life, and reliability. *Journal of Propulsion and Power*. 1987;3:76-83.
- [32] Sadeghi F, Jalalahmadi B, Slack TS, Raje N, Arakere NK. A Review of Rolling Contact Fatigue. *Journal of Tribology*. 2009;131.
- [33] Gu Z, Zhu C, Liu H, Du X. A comparative study of tribological performance of helical gear pair with various types of tooth surface finishing. *Industrial Lubrication and Tribology*. 2019;71:474-85.
- [34] Manieri F, Stadler K, Morales-Espejel GE, Kadiric A. The origins of white etching cracks and their significance to rolling bearing failures. *International Journal of Fatigue*. 2019;120:107-33.